Transparent Boundary Condition for Oseen-Frank Model. Application for NLC Cells With Patterned Electrodes

2015 J. Phys.: Conf. Ser. 605 012028

(http://iopscience.iop.org/1742-6596/605/1/012028)

Journal of Physics: Conference Series **605** (2015) 012028 doi:10.1088/1742-6596/605/1/012028

Transparent Boundary Condition for Oseen-Frank Model. Application for NLC Cells With Patterned Electrodes

I Orquín-Serrano[1], J Vijande[2], F R Villatoro[3], A Ferrando[4], P Fernández de Córdoba[1], and H Michinel[5]

[1]Instituto Universitario de Matemática Pura y Aplicada (IUMPA), Universidad Politécnica de Valencia (UPV), Camino de Vera s/n 46022 Valencia, Spain

[2]Departamento de Física Atómica, Molecular y Nuclear, Universidad de Valencia (UV) and IFIC (UV-CSIC), Valencia, Spain.

[3]Departamento de Lenguajes y Ciencias de la Computación, Universidad de Málaga (UMA), Málaga, Spain.

[4]Departament d'Óptica, Universitat de València (UV), 46100 Burjassot, Valencia, Spain.

[5]Optics Lab. University of Vigo, Facultade de Ciencias de Ourense, As Lagoas s/n. Ourense, 32004. Spain.

E-mail: `isorser@doctor.upv.es`

Abstract. In the present work a novel application of Transparent Boundary Conditions (TBC) to nematic liquid crystal cells (NLCC) with planar alignment and a patterned electrode is studied. This device is attracting great interest since it allows soliton steering by optically and externally induced waveguides. We employ the continuum Oseen-Frank theory to find the tilt and twist angle distributions in the cell under the one-constant approximation. The electric field distribution takes into account the whole 2D permittivity tensor for the transverse coordinates. Standard finite difference time domain methods together with an iterative method is applied to find an approximate solution to our coupled problem. A novel class of TBC is used to correctly define the boundary for both the distortion angle problem and the electric field distribution when using patterned electrodes. Thus, we achieve an important decrease of computational needs when solving this kind of problems and we are also capable of exploring weak anchoring conditions for NLCC.

1. Introduction

Nematic Liquid Crystal (NLC) Cells for lateral propagation are attracting much attention due, among other reasons, to their capability to form tunable reconfigurable waveguides. They can be formed by an external electric field [1] or by creating a self-consistent waveguide in bulk NLC [2]. These soliton induced waveguides can be used to implement all-optical switching and logic gating [3]. Tunable waveguide arrays can also be obtained in these kind of devices, in which all-optical switching phenomena [4] and optical multiband vector breathers [5] appear.

With respect to electrically induced waveguides, several NLC devices are being investigated. Many of them are based on using a patterned electrode to affect the molecules of the liquid crystal in such a way that the effective refractive index profile obtained yields a graded index waveguide inside the nematics [6]. Other dispositions, where two electrodes at different voltages are employed, are used for soliton routing [7, 8].

The problem of simulating the optical evolution in a stripped electrode device is a difficult one and involves necessarily a $2D+1$ anisotropic beam propagation method that at least takes into account the transverse anisotropy induced by the external electric field. Moreover, vectorial effects appear when the y component (see Fig. 1) of the external electric field is not negligible and pushes the molecules of the liquid crystal out of the propagation plane, making them twist. This implies changes in the polarization of the optical beam and also losses of the extraordinary solitonic beam. Some approximations are usually employed to avoid this complexity, obtaining good agreement with the experiments. One of these approximations is not considering the twist movement of the molecules. This approximation holds for low voltage values and for those cases where, although voltages are high, light moves far away from the vicinity of the patterned electrode where this twist is noticeable. Hard anchoring conditions for the orientational problem are usually employed. This boundary condition is realistic since the glass plates confining the NLC can be treated in such a way that tilt and twist angle are fixed at the boundary. However we can also work with a non-fixed value for the twist angle next to the glass plates allowing the tilt angle to be fixed. This is also realistic since a suitable treatment of the glass plates that allows this twist movement of the director at the boundary can be found.

In a weak anchoring situation the elastic constant depends on the position, in the proximity of the boundaries [9] and to determine the value of this surface (or anchoring) energy, small deviations close to the Friedericksz transition are usually considered [10]. The anchoring energy for deformations will be neglected as it is much lower than the corresponding energy for tilt deformations (tipically, one or even two orders of magnitude)[11]. We will show the numerical boundary treatment in this case, what could be used for further numerical research looking for better characterizing the boundary influence on the elastic constants under weak anchoring conditions as it was done in some studies in the past[12].

This is the regime we want to show in this paper, where transparent boundary conditions for the twist angle will be necessary in the boundary next to the glass plates. These simulations widens our knowledge of what is actually happening in the area closest to the electrode.

This paper is organized as follows: section 2 presents the physical model, section 3 shows the numerical treatment that allows us to approximate the solution of the problem using the boundary condition explained in section 4. Some results of our numerical model are presented in section 5 for different electrode configurations and finally our conclusions are presented in section 6.

2. Physical Model

We want to simulate a NLC device made of two glass plates containing commercial NLC E7 in between indium tin oxide transparent electrodes connected to the glass plates to apply an external voltage to the liquid crystal. It can be seen in Fig. 1 the geometrical properties of such a device; z coordinate stands for the propagation axis while x and y represent transverse spatial dimensions. Tilt angle (θ) appears with any movement of the director along a plane perpendicular to the yz plane. Twist angle (φ) is defined in zy plane and holds for the twist deformations of the director. Planar alignment imposes director orientation nearly parallel to the glass plates, i.e., small tilt angle ($\theta = 2°$). $V = 0$ is applied to the lower electrode affecting the whole glass plate. Upper one is thinner and doesn't affect the whole upper glass plate, so we will refer to it as the stripped electrode, where $V \neq 0$ is applied. This physical configuration makes the numerical boundary difficult to work with because of its undefinition where the upper electrode doesn't influence the liquid crystal orientation. This discontinuity on the upper boundary, forced by the discontinuous electrode makes appear an y component for the electric field, such a component being responsible for the twist angle to appear in the proximities of

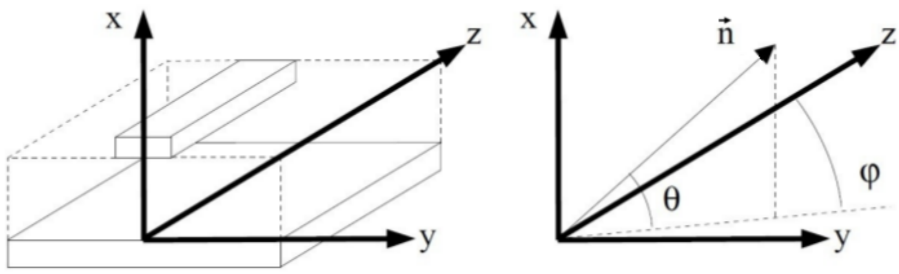

Figure 1. Sketch of the nematic liquid crystal device with patterned electrode (left) and notation for the planar alignment in the cell (right).

the stripped electrode. So a complete molecular reorientation is needed to explain both angle distributions. The whole orientational problem has already been solved in an iterative way for different NLC configurations where no discontinuous electrode is taken into account [13]. We extend this iterative method to the two dimensional case and we also present the two dimensional electric field distribution in those cases where tilt and twist angle distributions affect the electric field imposed by the electrodes, i.e., taking into account the whole 2D permittivity tensor.

2.1. Electric field distribution

We start from the Maxwell equations

$$\left.\begin{array}{r} \nabla D = 0 \\ D = \epsilon E \\ E = -\nabla V \end{array}\right) \rightarrow \nabla\left(\bar{\epsilon}\nabla V\right) = 0, \tag{1}$$

where ϵ_{ij} with $i = x, y, z$ and $j = x, y, z$ are permittivity tensor terms, given by

$$\epsilon = \begin{pmatrix} \epsilon_\perp + \Delta\epsilon \sin^2\theta & \Delta\epsilon \sin\theta\cos\theta\sin\varphi \\ \Delta\epsilon\sin\theta\cos\theta\sin\varphi & \epsilon_\perp + \Delta\epsilon\cos^2\theta\sin^2\theta \end{pmatrix}, \tag{2}$$

where $\epsilon_\perp$ is the perpendicular (to the glass plates) component of the permittivity and $\Delta\epsilon = \epsilon_\parallel - \epsilon_\perp$ is the birefringence of the medium. Tilt $(\theta(x,y))$ and twist $(\varphi(x,y))$ angles depend only on these transverse coordinates. By doing so we are uncoupling the z coordinate therefore obtaining a static transverse distribution. We also consider negligible any dependence on z of the functions, i.e. $V(x,y,z) = V(x,y)$, $\frac{\partial V}{\partial z} = 0$, $\frac{\partial^2 V}{\partial z^2} = 0$, $\frac{\partial^2 V}{\partial y \partial z} = 0$, $\frac{\partial^2 V}{\partial x \partial z} = 0$, $\frac{\partial \theta}{\partial z} = 0$, $\frac{\partial \varphi}{\partial z} = 0$.

Substituting the dielectric tensor expressions in Eq. (1) and not considering any dependence on the z coordinate one obtains for the static two dimensional problem in the transverse plane,

$$a_1\frac{\partial^2 V}{\partial x^2} + a_2\frac{\partial^2 V}{\partial y^2} + a_3\frac{\partial^2 V}{\partial x \partial y} + a_4\frac{\partial V}{\partial x} + a_5\frac{\partial V}{\partial y} = 0, \tag{3}$$

with

$$a_1 = \frac{1}{\Delta x^2}\left(\epsilon_\perp + \Delta\epsilon\sin^2\theta\right), \tag{4}$$

$$a_2 = \frac{1}{\Delta y^2}\left(\epsilon_\perp + \Delta\epsilon\cos^2\theta\sin^2\varphi\right), \tag{5}$$

$$a_3 = \frac{1}{4\Delta x \Delta y}\Delta\epsilon\sin(2\theta)\sin\varphi, \tag{6}$$

$$a_4 = \frac{1}{2\Delta x}\left(\Delta\epsilon\left(\cos(2\theta)\sin\varphi\frac{\partial\theta}{\partial y}+\cos\theta\sin\theta\left(\cos\varphi\frac{\partial\varphi}{\partial y}+2\frac{\partial\theta}{\partial x}\right)\right)\right), \tag{7}$$

$$a_5 = \frac{1}{2\Delta y}\left(\Delta\epsilon\left(\left(\cos^2\theta\sin\varphi-\sin^2\theta\sin\varphi\right)\frac{\partial\theta}{\partial x}\right.\right. \tag{8}$$

$$\left.\left.-\sin(2\theta)\sin^2\varphi\frac{\partial\theta}{\partial y}+\cos\theta\cos(\varphi)\sin\theta\frac{\partial\varphi}{\partial x}+\cos^2\theta\sin(2\varphi)\frac{\partial\varphi}{\partial y}\right)\right). \tag{9}$$

This is the equation we solve to obtain the electric field distribution. Notice that the dielectric tensor is responsible of the graded index profile which appears in the Beam Propagation Method, this is the way this whole static problem is coupled with the optical problem, which we are not studying here.

Finite Difference method is used to approximate this equation. Centered second order differences are employed for approximating the differential operators. Newton-Raphson method is used to solve the nonlinear equations of the finite difference scheme.

2.2. Elastic distortion angles distribution

As it was mentioned before, Oseen-Frank theory is employed to describe the molecular orientation in the NLC cell [14]. The total free energy of the liquid crystal is calculated to obtain its minimum via the Euler Lagrange theory. All three energy terms are considered in this model: the electric energy due to the external voltage, the electric energy due to the optical beam propagating inside the cell, and the elastic distortion energy.

The elongated molecules from the NLC feel any electric field due to its electric polarity, so they react changing its orientation so that it is aligned with the total electric field. Thus, molecules orientation is defined by the director vector $\overline{n} = (\sin\theta, \cos\theta\sin\varphi, \cos\theta\cos\varphi)$.

The distortion energy per volume unit considers three different types of distortion, each one with different elastic constants K. Under *one constant approximation*, all three elastic constants, related to different molecular distortions, are considered to be equal resulting in a more simplified equation. Minimizing the energy density can be done by transforming this problem to the solution of a partial differential equation via Euler-Lagrange theory, yielding:

$$\begin{aligned}
&-K\left(\frac{\partial^2\theta}{\partial x^2}+\frac{\partial^2\theta}{\partial y^2}\right)+\sin(2\theta)\left[-\frac{K}{2}\left(\frac{\partial\varphi}{\partial x}^2+\frac{\partial\varphi}{\partial y}^2\right)\right.\\
&+\epsilon_0\left(-\frac{1}{2}\left(\Delta\epsilon^s|E_x^s|^2+\Delta\epsilon^o|E_x^o|^2\right)+\frac{\Delta\epsilon^s}{4}|E_y^s|^2(1-\cos(2\varphi))\right.\\
&\left.\left.+\frac{1}{2}\Delta\epsilon^o\sin^2\varphi|E_y^o|^2\right)\right]-\frac{1}{2}\epsilon_0\cos(2\theta)\sin\varphi\left(\Delta\epsilon^o\left(E_y^{o*}E_x^o+E_x^{o*}E_y^o\right)\right.\\
&\left.+2\Delta\epsilon^s E_x^s E_y^s\right)=0,
\end{aligned} \tag{10}$$

and

$$\begin{aligned}
&K\cos\theta\left[\cos\theta\left(\frac{\partial^2\varphi}{\partial x^2}+\frac{\partial^2\varphi}{\partial y^2}\right)-2\sin\theta\left(\frac{\partial\theta}{\partial x}\frac{\partial\varphi}{\partial x}+\frac{\partial\theta}{\partial y}\frac{\partial\varphi}{\partial y}\right)\right]\\
&+\frac{1}{2}\epsilon_0\cos^2\theta\sin(2\varphi)\left(\Delta\epsilon^o|E_y^o|^2+\Delta\epsilon^s|E_y^s|^2\right)\\
&+\frac{1}{4}\epsilon_0\cos\varphi\sin(2\theta)\left(\Delta\epsilon^o\left(E_y^{o*}E_x^o+E_x^{o*}E_y^o\right)\right)\\
&+2\Delta\epsilon^s E_x^s E_y^s=0,
\end{aligned} \tag{11}$$

that will allow us to solve $\theta(x, y)$ and $\varphi(x, y)$ respectively. Typical values we use for the magnitudes involved are $K = 12\times10^{-12}$ N, $\Delta\epsilon^s = \epsilon_\parallel^s - \epsilon_\perp^s = 19.6 - 5.1$, $\Delta\epsilon^o = \epsilon_\parallel^o - \epsilon_\perp^o = n_\parallel^2 - n_\perp^2 = 1.69^2 - 1.50^2$.

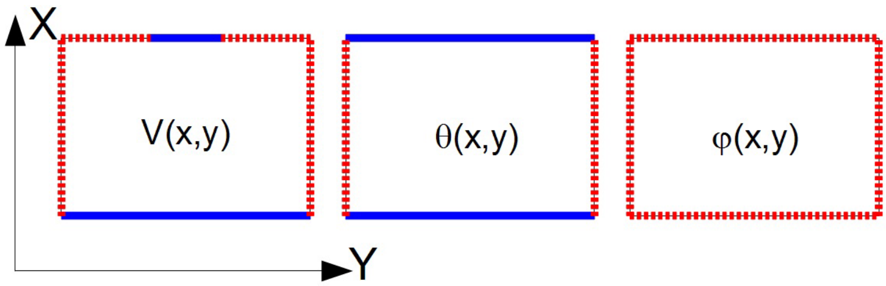

Figure 2. Numerical domain for all three differential equations. Blue solid lines represent hard anchoring condition while red dotted lines hold for transparent boundary condition.

3. Numerical Model

All three equations (3, 10 and 11) are approximated by a finite difference method consisting of difference operators which approximates the differential operators to second order, both for first and second derivatives. The corresponding nonlinear boundary value problems require the use of an iterative method such as Newton-Raphson ([15]) in order to find an approximate solution. Following the notation of [16] we write the difference equation which approximates eq. (3)

$$\begin{aligned} a_{1_{j,k}}\delta_x^2 V_{j,k} + \quad & a_{2_{j,k}}\delta_y^2 V_{j,k} + a_{3_{j,k}}(\delta_{0y}(\delta_{0x}V_{j,k})) \\ + \quad & a_{4_{j,k}}\delta_{0x}V_{j,k} + a_{5_{j,k}}\delta_{0y}V_{j,k} = 0, \end{aligned} \tag{12}$$

being $\delta_x^2 V_{j,k} = V_{j-1,k} - 2V_{j,k} + V_{j+1,k}$ and $\delta_y^2 V_{j,k} = V_{j,k-1} - 2V_{j,k} + V_{j,k+1}$ the second order approximations to the second spatial derivatives and $\delta_{0x}V_{j,k} = V_{j+1,k} - V_{j-1,k}$ and $\delta_{0y}V_{j,k} = V_{j,k+1} - V_{j,k-1}$ the second order approximations to the first spatial derivatives. Notice that difference operators δ_{0x} and δ_{0y} commute. Coefficients $a_{i_{j,k}}$ represent the discretized version of the respective coefficients of eq. (3). It can be seen that coefficients $a_{1_{j,k}}, a_{2_{j,k}}$ and $a_{3_{j,k}}$ are point approximations while $a_{4_{j,k}}$ and $a_{5_{j,k}}$ require the application of difference operators to the angle derivatives appearing in those coefficients. Thus the boundary condition will appear also in these coefficients.

We can rewrite eq. (12) in a more clear way

$$\begin{aligned} & A_{NW_{j,k}}V_{j-1,k-1} + A_{N_{j,k}}V_{j,k-1} + A_{NE_{j,k}}V_{j+1,k-1} \\ + \quad & A_{W_{j,k}}V_{j-1,k} + A_{P_{j,k}}V_{j,k} + A_{E_{j,k}}V_{j+1,k} \\ + \quad & A_{SW_{j,k}}V_{j-1,k+1} + A_{S_{j,k}}V_{j,k+1} + A_{SE_{j,k}}V_{j+1,k+1} = 0 \end{aligned} \tag{13}$$

where the coefficients stand for the location of the nodes in the discrete molecule of the difference method. This is a nine point molecule whose coefficients are $A_{NW_{j,k}} = a_{3_{j,k}}$, $A_{N_{j,k}} = a_{2_{j,k}} - a_{5_{j,k}}$, $A_{NE_{j,k}} = -a_{3_{j,k}}$, $A_{W_{j,k}} = a_{1_{j,k}} - a_{4_{j,k}}$, $A_{P_{j,k}} = -2a_{1_{j,k}} - 2a_{2_{j,k}}$, $A_{E_{j,k}} = a_{1_{j,k}} + a_{4_{j,k}}$, $A_{SW_{j,k}} = -a_{3_{j,k}}$, $A_{S_{j,k}} = a_{2_{j,k}} + a_{5_{j,k}}$, $A_{SE_{j,k}} = a_{3_{j,k}}$ accounting for the north-west, north, north-east, west, central, east, south-west, south and south-east nodes respectively. This is a very convenient notation since the matrix of coefficients of eq. (13) and the matrix representing the jacobian of that difference functional coincides.

Equations (10) and (11) are solved analogously using second order difference operators and Newton-Raphson method. Notice that the numerical scheme of these equations yields a five-point molecule instead of the nine-point molecule appearing in eq. (13) due to the crossed second derivative approximation.

The main drawback of this formalism is that an iterative scheme is needed to reach an autoconsistent solution since equations (3), (10) and (11) are coupled. An iterative scheme can

Journal of Physics: Conference Series **605** (2015) 012028 doi:10.1088/1742-6596/605/1/012028

be used to obtain the solution to this coupled problem. First an iterative loop will find the auto consistent solution of the approximated equations of (10) and (11) and then use this solution to find the electric field distribution using (3). Then other iterative loop is needed for finding an autoconsistent solution of both problems the electric and the angular one. Thus, two nested iterative loops scheme have been used to find the whole autoconsistent solution.

4. Transparent Boundary Condition

All three differential equations we solve have different boundary conditions as it can be seen in Fig. 2. First, the calculation for the external electric potential applied over the nematics requires hard anchoring condition wherever we have an electrode fixing the voltage. Where no electrode is located we use transparent boundary condition since it allows no restrictions over the voltage value at the boundary, which is a realistic boundary. Second, with respect to the tilt angle distribution, $\theta(x, y)$ we use hard anchoring condition for the x boundary, since that is the area where the nematics is limited by the glass plate, which usually has a rubbing treatment to fix the tilt angle to a low value, typically $\theta = 2°$, with no possibility of movement in this boundary. Finally, twist angle $\varphi(x, y)$ is not fixed in the x boundary, since the glass plates allows twist movement of the molecules, parallel to the glass plates, after appropriate treatment of the surface. It can be seen in Fig. 2 that TBC are used for all three problems in the y boundary allowing a finite extent in this transverse coordinate of such device. Gratings can be simulated by employing periodic boundary conditions in y boundary.

TBC allow us to predict which has to be the value of the function at the boundary using the information we have in the interior domain. From the middle 70's on much work has been done to develop a total non reflecting boundary condition for the Schrödinger equation ([17, 18, 19, 20, 21, 22, 23, 24, 25]). Absorbing boundary conditions are still being studied and its application to dispersive waves phenomena [26] or its behavior with semilinear parabolic equations [27] have been published recently. Different approaches have been proposed, both analytical and numerical, but the work of G. R. Hadley has become one of the most popular results published in this topic because of its easy implementation at the time it offers very good results. Hadley's work presents the derivation of a TBC for the Schrödinger equation, based on physical considerations about the energy flow through the numerical boundaries [28, 29]. We use similar mathematical considerations which allow us to predict the value of the function at the boundary. In this work we extend the use of this TBC to other differential equations. Let us show the calculation of this transparent boundary condition with an example for the external electric potential $V(x, y)$. Let $V_{j,k}$ be the discretized values $V(j\Delta x, k\Delta y)$ where $2 \leq j \leq N_X - 1$ and $2 \leq k \leq N_Y - 1$, N_X and N_Y being the number of unknowns in the x and y direction respectively.

Consider a fixed value for j in the external electric potential case, say $j = N_X/2$. Calculate the set of values $c_{y_{j,k}} = \frac{V_{j,k}}{V_{j,k+1}}$, as the quotient of consecutive values in the y direction. Index k ranges from 2 to $N_Y - 1$, being N_Y the number of nodes in the y direction (with $N_Y - 2$ unknowns). Notice that boundary values in the y direction in this set are $V_{j,1}$ and V_{j,N_Y}. We could guess the values of the y boundary if we got a value for $c_{y_{j,1}}$ and $c_{y_{j,N_Y-1}}$. Of course this set of values $c_{y_{j,k}}$ depend on the value function. In order to obtain these quantities at the boundaries we use a linear extrapolation, saying $c_{y_{j,1}} = 2 \cdot c_{y_{j,2}} - c_{y_{j,3}}$ and $c_{y_{j,N_Y-1}} = 2 \cdot c_{y_{j,N_Y-2}} - c_{y_{j,N_Y-3}}$. Depending on the solution shape at the boundary we must evaluate the convenience of using other higher order extrapolation in order to obtain better accuracy. Thus we can say $V_{j,1} = V_{j,2} \cdot c_{y_{j,1}}$ and $V_{j,N_Y} = V_{j,N_Y-1}/c_{y_{j,N_Y-1}}$. We calculate all transparent boundaries in a similar way, using the extrapolated values of the convenient quotient for each case. These transparent boundary values for the external electric potential $V_{j,k}$ are used in Eq. (3). Notice that not all the values for the quotient vector $c_{x_{j,k}}$ (or analogously $c_{y_{j,k}}$) are employed.

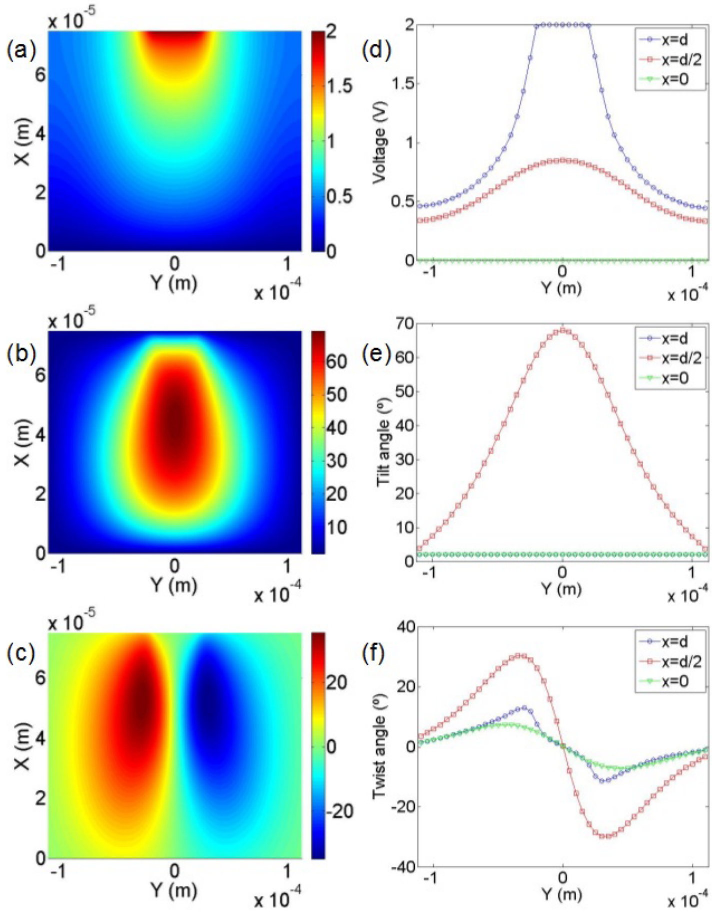

Figure 3. (a), (b) and (c) Show potential, tilt and twist angle distribution for $V = 2$ V respectively. (d), (e) and (f) Show three different sections of (a), (b) and (c) respectively. Blue circles, red squares and green triangles represent cuts of the three dimensional representation on the left around $x = d$, $x = d/2$ and $x = 0$ respectively. Notice that some curve might be overlapping the axes or other curve.

5. Results

5.1. One single electrode

The single electrode device represented in Fig. 1 has been used experimentally in order to guide nematicons in planar devices [30]. Fig. 3 shows the solution for the electric potential, the tilt angle and twist angle for $V = 2$ V. There it can be seen the effect of the transparent boundary condition. Although optical power affects the molecular orientation (as it can be seen in equations 10 and 11, we perform simulations for different voltages with no optical power, so that it doesn't appear any other electric excitacion than the external field. It can be seen in Fig. 4 the effect of the voltage on both the tilt and the twist angle. Both angles show different behavior: tilt angle changes more abruptly that twist angle. Changes begin at voltage $V = 1$ V since that supposes the minimal amount of energy necessary to start moving the LC molecules, what is known as the Friedericksz threshold. Models which don't take into account twist angle shouldn't be appropriate for describing voltages above one volt since from then on twist angle is no longer negligible. To our knowledge this is the first time that transparent boundary conditions are applied to these equations.

This one electrode device has already been studied to show the lateral propagation of a soliton

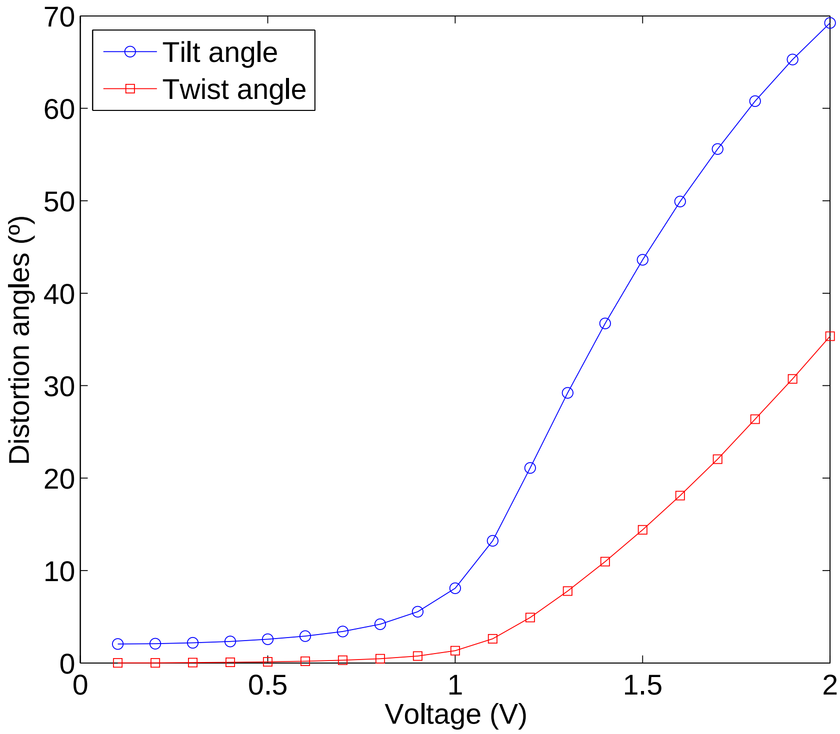

Figure 4. Voltage dependence over the peak values for the tilt and twist angles. These are the results of 200 simulations raging from $V = 0.01$ V to $V = 2$ V.

inside the NLCC. However it is said that it is necessary to extend artificially the computational domain in order to solver the electric field distribution inside the cell since nothing is known from the solution at the boundary [30]. The idea is setting a fixed value for the solution in an artifical boundary far enough from the real one so that one can say that it doesn't affect the solution inside the original numerical domain. Our TBC permits us to avoid this artifical extension of the 2D numerical domain, lowering this way the computational needs to solve the whole coupled problem.

5.2. Two different electrodes with gap in between

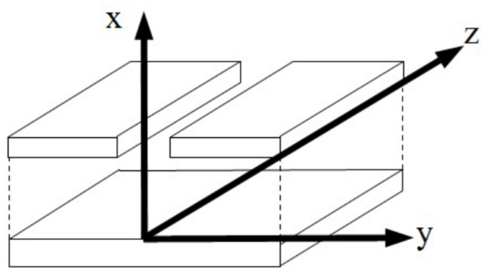

Figure 5. NLC Device with two different electrodes in the upper area.

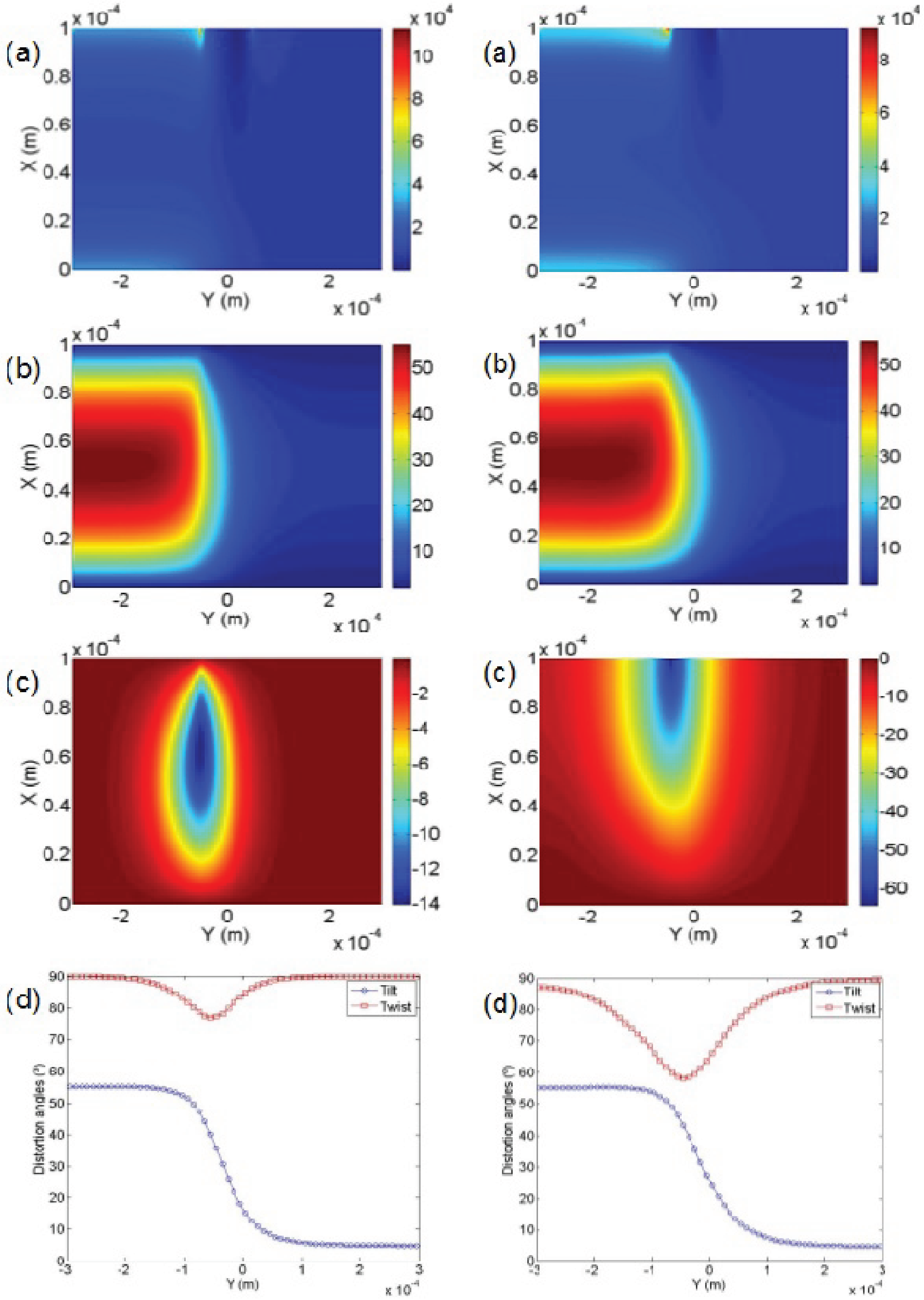

Figure 6. Solution for a two electrode device with Dirichlet boundary conditions at x boundaries (on the left) and using transparent boundary conditions at x boundaries for twist angle (on the right). Voltages are $V_1 = 1.5$ V and $V_2 = 0.7$ V. (a) Electric field, (b) tilt angle and (c) twist angle. Plot (d) show cross sections of both angles, tilt and twist, at $x = d/2$.

NLC Devices for lateral propagation and two electrodes with a gap in between have been studied for demonstrating tunable refraction and reflection of a soliton inside the nematics [31]. Fig. 5 shows which is the device we are referring to. Hard anchoring boundary conditions have been employed for the distortion angles, tilt and twist, in the x boundary since these values are fixed experimentally using a rubbing technique of the glass plates. Tilt angle is always fixed at the boundary since it is very difficult to allow a tilt movement of the molecules in a plane perpendicular to the glass plate there. However other boundary conditions are also realistic for the twist angle. Particularly, the *hybrid* case where the $x = 0$ boundary is defined by a hard anchoring condition and the $x = d$ boundary is transparent, allowing the molecules to twist at the boundary $x = d$, is also realistic. We study this case as a clear example of the use of our transparent boundary conditions. Notice that also transparent boundary conditions are employed for all three problems (V(x,y), $\theta(x, y)$ and $\varphi(x, y)$) in the y boundaries, allowing thus to study a single device of a finite extent.

In the device described in [31] the electrodes are used to create an effective index distribution so that it affects the nematicon trajectory in different ways. We have performed the simulations of such device in two different scenarios: total anchoring condition in the x boundary, and the hybrid case mentioned before. The results are illustrated in Fig. 6, where we show the difference among both configurations. No changes in tilt angle distribution are observed since the calculation remains the same in both cases. However, twist angle distributions differ because of the effect of the transparent boundary condition applied in $x = d$. In fact, the amplitude of the twist angle in the latter case is bigger since it is not restricted by the boundary. This also affects the electric field distribution which reaches lower values in that boundary.

The application of a TBC to NLC devices allow us to study new configurations where weak anchoring conditions are relevant. For example in-plane movements of the molecule (those corresponding to the twist deformation) at the boundary are common in twisted nematic liquid crystal cells which may be used as displays, for example.

6. Conclusions

We have developed a realistic two dimensional numerical model for the coupled problem of finding the electric field distribution in a planar NLC cell considering the effects of both the tilt and twist director deformations. Oseen-Frank theory for the director distribution has been employed. To our knowledge, transparent boundary conditions are applied for each differential equation for the first time, thus avoiding time-consuming codes where artificial extension of the numerical domain were necessary to simulate devices with patterned electrodes correctly. The use of TBC in the y direction allow us to simulate one single electrode device properly. In the x direction TBC are only used for the twist deformation in the single electrode device. It reaches non negligible values close to the upper boundary where the patterned electrode is located. Other devices have been simulated to show the robustness of our code, for example a two electrode device with different voltages has been calculated. A TBC for the twist deformation at all four boundaries has been used to show the differences between the code already solved in the literature and our code, which enlightens a bit more the weak anchoring situation (for the twist angle) in those kind of devices.

Acknowledgments

A.F. thanks Ministerio de Ciencia e Innovación of Spain by its financial support (TIN2006-12890 and TEC2010-1532). F.R.V. thanks Ministerio de Ciencia e Innovación (MICINN) of Spain by its financial support (TIN2009-12359 and MTM2010-19969). P.F.C. thanks MICINN of Spain by its financial support (TIN2009-12359).

References

[1] Peccianti M, De Rossi A, Assanto G, De Luca A, Umeton C and Khoo I C 2000 *Applied Physics Letters* **77**
[2] Peccianti M and Assanto G 2001 *Opt. Lett.* **26** 1690–1692
[3] Peccianti M, Conti C, Assanto G, De Luca A and Umeton C 2002 *Applied Physics Letters* **81**
[4] Fratalocchi A, Assanto G, Brzdkiewicz K A and Karpierz M A 2005 *Applied Physics Letters* **86** 051112
[5] Fratalocchi A, Assanto G, Brzdakiewicz K A and Karpierz M A 2005 *Opt. Lett.* **30** 174–176
[6] Beeckman J, Neyts K and Haelterman M 2006 *Journal of Optics A: Pure and Applied Optics* **8** 214
[7] Peccianti M, Dyadyusha A, Kaczmarek M and Assanto G 2008 *Phys. Rev. Lett.* **101**(15) 153902
[8] Kivshar Y 2006 *Nature Phys.* **2** 729
[9] Alexe-Ionescu A L, Barberi R, Barbero G and Giocondo M 1994 *Phys. Rev. E* **49**(6) 5378–5388
[10] Sodré N, Zola R S, Lenzi E K and Evangelista L R 2006 *Rev. Mex. Rev. Mex. de Física S* **52** 80–84
[11] Jéróme B 2008 *Handbook of Liquid Crystals* (Wiley-VCH Verlag GmbH) pp 535–548
[12] Allen M P and Frenkel D 1988 *Phys. Rev. A* **37**(5) 1813–1816
[13] Wang Q, He S, Yu F and Huang N 2001 *Optical Engineering* **40** 2552–2557
[14] Khoo I C 2006 *Liquid Crystals: Physical Properties and Nonlinear Optical Phenomena* (Cambridge University Press)
[15] Press W H, Teukolsky S A, Vetterling W T and Flannery B P 2007 *Numerical Recipes: The Art of Scientific Computing* (John Wiley & Sons, Inc.)
[16] Thomas J W 1995 *Numerical Partial Differential Equations* (Springer, New York)
[17] Engquist B and Majda A 1977 *Math. Comp* **31** 629–651
[18] Grote M and Keller J 1995 *SIAM Journal on Applied Mathematics* **55** 280–297
[19] Hagstrom T, Warburton T and Givoli D 2010 *Journal of Computational and Applied Mathematics* **234**
[20] Baskakov V and Popov A 1991 *Wave Motion* **14** 123 – 128
[21] Lubich C and Schädle A 2002 *SIAM Journal on Scientific Computing* **24** 161–182
[22] Kuska J P 1992 *Phys. Rev. B* **46**(8) 5000–5003
[23] Menza L D 1996 *Applied Mathematics Letters* **9** 55 – 59
[24] Sch A 2002 *Wave Motion* **35** 181 – 188
[25] Arnold A, Ehrhardt M and Sofronov I 2003 *Commun. Math. Sci.* **1** 501–556
[26] Lindquist J M, Neta B and Giraldo F X 2012 *Applied Mathematics and Computation* **218** 6666 – 6676
[27] Sun Z Z, Wu X, Zhang J and Wang D 2012 *Applied Mathematics and Computation* **218** 5187 – 5201
[28] Hadley G R 1991 *Opt. Lett.* **16** 624–626
[29] Hadley G 1992 *Quantum Electronics, IEEE Journal of* **28** 363–370
[30] Beeckman J, Chaubiska K and Neyts K 2006 *Ferroelectrics* **344** 225–231
[31] Peccianti M, Dyadyusha A, Kaczmarek M and Assanto G 2006 *Nat Phys* **2** 737–742